Sedimentation and levitation of catalytic active colloids

Virginia Carrasco Fadanelli, Ivo Buttinoni

Article - Version of Record

Letter

Sedimentation and levitation of catalytic active colloids

V. Carrasco-Fadanelli * and I. Buttinoni

Institute of Experimental Colloidal Physics, Department of Physics, Heinrich-Heine-Universität Düsseldorf, 40225 Düsseldorf, Germany

(Received 31 May 2022; accepted 27 January 2023; published 13 February 2023)

Gravitational effects in colloidal suspensions can be easily turned off by matching the density of the solid microparticles with the one of the surrounding fluid. By studying the motion of catalytic microswimmers with tunable buoyant weight, we show that this strategy cannot be adopted for active colloids with asymmetric mass distribution. If the average buoyant weight decreases, pronounced accumulation at the top wall of a sample cell is observed due to a counteralignment of the swimming velocity with the gravitational field. Even when the particles reach a flat wall, gravitational torques still determine the properties of the quasi-two-dimensional active motion. Our results highlight the subtle role of gravity in active systems.

DOI: 10.1103/PhysRevResearch.5.L012018

Active Brownian particles are a new generation of colloids, which undergo self-propulsion rather than being in thermal equilibrium with their liquid environment [1–3]. They have been receiving much attention as model systems for living matter [4], microvehicles for technological applications (e.g., in the realm of drug delivery) [5,6], and building blocks for the design of new materials with self-sustaining properties [7–10].

Many of the existing synthetic microswimmers take advantage of interfacial phenomena such as phoresis and osmosis to achieve self-propulsion [11]. In short, patchy colloids can generate local asymmetric conditions (e.g., thermal or chemical gradients) that, in turn, give rise to slip flows and directed motion [12]. The most widespread example—also of main interest for the present study—is that of spherical particles half-coated with a layer of platinum (Pt) and suspended in hydrogen peroxide (H_2O_2) enriched solutions [13–17]. The platinum cap acts as a catalyst and locally decomposes the "fuel" into H_2O and O_2 leading to autophoretic swimming velocities that increase with the bulk concentration of hydrogen peroxide, $[H_2O_2]_\infty$. Importantly, in the absence of confinements or external fields, the velocity vector is always oriented along the axis linking the poles of the two hemispheres and rotates together with the particle.

To date, experiments with synthetic active particles are almost entirely limited to (quasi) two-dimensional (2D) systems, with only few exceptions [17–19]. Self-propelling colloids heavier than the solvent sediment towards the bottom of the container (*positive gravitaxis*), although fast bottom-heavy [20,21] and asymmetric [22] active particles may also levitate (*negative gravitaxis*) due to a counteralignment of the velocity vector with the gravitational field. Polarization of the swimming velocity against gravity has been also predicted and observed in suspensions of active particles with homogenous density distribution [23–25]. Positive and negative gravitaxis have been studied as a function of the swimming velocity and size [20,21], but we are not aware of experimental studies addressing specifically the role of the buoyant weight—which is paramount to achieve zero effective gravity—of the self-propelling particles. Likewise, existing studies of catalytic self-propulsion near flat confinements only address the case of "heavy" colloids; they unanimously suggest that, in the presence of underlying substrates, active colloids exhibit a steady motion with a fixed distance from the substrate and an orientation that depends on the relaxation time linked to the wall-interaction torque [14,15,26–29].

In this Letter, we fine-tune the buoyant weight of catalytic microswimmers and study how it influences the active motion in bulk and near solid surfaces. Buoyancy plays a key role in the direction of particle migration, i.e., whether the colloids sink to the bottom substrate, levitate towards the top wall or remain in the bulk of the sample cell. Experiments and Brownian dynamics simulations reveal that, if the average buoyant weight becomes close to zero, accumulation takes place almost entirely at the top wall due to a "residual" gravitational torque. Once the particles reach a substrate, they undergo an oscillatory motion (in the direction of gravity) with a frequency and amplitude that depend on both the swimming velocity and buoyant weight.

We first fabricate patchy particles by drying a diluted suspension of spherical fluorescent polystyrene (PS) beads (Microparticles GmbH, radius $R = 1.4$ μm) onto a precleaned microscope slide (Thermo Scientific) and later sputtering a layer of platinum (thickness, $\lambda = 4 \pm 0.5$ nm) with 90° glancing angle to coat the exposed hemispheres. The particles are then detached from the glass substrate via sonication in milliQ water and dispersed in H_2O-D_2O-H_2O_2 solutions. The sample cell [Hellma Analytics, Flow cell 137-QS, Suprasil quartz glass, 1 mm H × 35 mm L × 9 mm W, see sketch in Fig. 1(a)] is filled with the mixture using a pipette and the out- and inlets are sealed with parafilm. We measure the particle

*carrasv@hhu.de

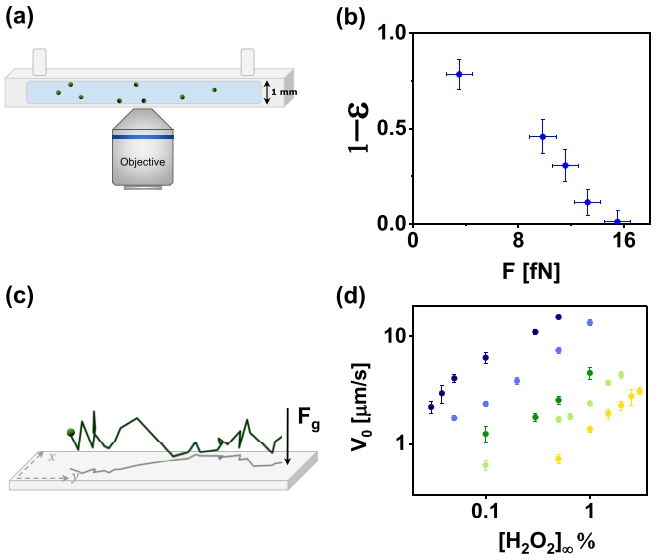

FIG. 1. (a) Sketch of the experimental setup. A quartz cell is filled with a suspension of active particles in H_2O-D_2O-H_2O_2 solutions and imaged from below using an inverted microscope. (b) Fraction of "passive" particles ($[H_2O_2]_\infty = 0\%$) in the bulk of the cell, $1-\varepsilon$, one hour after injection, plotted as a function of the buoyant weight F. The data are in agreement with simulations of "passive" Brownian particles (not shown). (c) Experimental trajectories in 2D (gray line) and 3D (green line) of an active particle close to the bottom substrate. Gravity points in the z direction. The mean velocity in the xy plane (plane parallel to the substrate) is obtained by fitting the 2D-MSD. (d) V_0 vs $[H_2O_2]_\infty$ for five different buoyant weights. From blue to yellow: $F = 15.52$ fN, $F = 13.25$ fN, $F = 11.57$ fN, $F = 9.85$ fN, $F = 3.51$ fN.

volume fraction ϕ by injecting a suspension of "passive" colloids ($[H_2O_2]_\infty = 0$ %), letting the particles entirely sediment onto the bottom wall, and taking pictures of non-overlapping regions using an inverted fluorescence microscope (Olympus IX73), in order to count the number of particles and extrapolate $\phi \approx 0.005\%$ v/v. We then use the exact same particle concentration in "active experiments" ($[H_2O_2]_\infty > 0$ %).

Each colloid is subjected to two forces: A gravitational weight, which is the sum of the weights of the PS-sphere and Pt-coating, i.e.,

$$\mathbf{F}_g = \left[\tfrac{4}{3}\pi R^3 \rho_{ps} + 2\pi\lambda R^2 \rho_{pt}\right]\mathbf{g}, \quad (1)$$

and a buoyant force

$$\mathbf{F}_b = -\tfrac{4}{3}\pi R^3 \rho_s \mathbf{g}. \quad (2)$$

Here, $\mathbf{g}$ is the gravity acceleration (pointing towards the bottom wall), and $\rho_{ps} = 1.05$ g/cm^3, $\rho_{pt} = 21.45$ g/cm^3 and ρ_s are the densities of the polystyrene particles, platinum cap and solvent, respectively. In our experiments, the coating contributes to approximately 10% of the total gravitational weight. The addition of D_2O allows us to vary ρ_s and, as such, achieve a buoyant force that almost entirely counteracts $\mathbf{F}_g$ ($[D_2O] = 100\%$). Within the experimental timescale of one hour, this leads to nearly weightless colloids (buoyant weight, $\mathbf{F} = \mathbf{F}_g + \mathbf{F}_b \simeq 0$), as shown by the large fraction $(1-\varepsilon)$ of particles staying in the bulk [Fig. 1(b); note, however, that at longer times the particles will eventually sediment]. We shall see that this conclusion is valid only in the absence of activity.

Soon after injection, the catalytic active colloids undergo self-propulsion in bulk with the PS-hemispheres heading; some go to the top wall of the cell, some to the bottom wall and others remain in the bulk. After a particle reaches a surface, it never swims back to the bulk. We first record images of active colloids swimming on the bottom substrate at 5 frames per second by means of an inverted fluorescence microscope and a CMOS camera, and extract the xy trajectories [grey trajectory in Fig. 1(c)] using Matlab scripts. The mean swimming velocity in xy, which we denote as V_0, is obtained by fitting mean squared displacement (MSD) of approximately 15 particles using a 2D active Brownian motion (ABM) model, where the particles are assumed to rotate and translate in the xy plane (see the Supplemental Material [30]). We repeated the measurements for each sample after approximately one hour of deposition to ensure that the average swimming velocity is still the same. As opposed to all existing experiments, V_0 is not only a function of $[H_2O_2]_\infty$, but also the ratio between H_2O and D_2O, possibly due to the higher stability of deuterium peroxide [31]. As the concentration of D_2O increases, more hydrogen peroxide is needed to obtain the same swimming velocity, as illustrated by the different colours (from dark blue, $[D_2O] = 0\%$, to yellow, $[D_2O] = 100\%$) of the experimental data in Fig. 1(d). We often observe a linear growth of V_0 as a function of the fuel concentration, although a more complex dependence is reported in H_2O-H_2O_2 mixtures for small values of $[H_2O_2]_\infty$ (a plot of the data for $[D_2O] = 0\%$ and a broader range of $[H_2O_2]_\infty$ is given in the Supplemental Material [30]). V_0 is approximately the same regardless of the cell wall (bottom vs top) they are close to.

By controlling $[D_2O]$ and $[H_2O_2]_\infty$, we look at the ratio of particles that accumulate at the top (ε^T) and bottom (ε^B) walls as a function of F (V_0), while keeping V_0 (F) constant ($\varepsilon = \varepsilon^B + \varepsilon^T$). ε^B and ε^T are not steady-state quantities, but rather calculated as the average number of particles (within the depth of field of the 10x objective, DOF = 10.54 μm) at the bottom/top wall one hour after injection, divided by the total amount of particles injected in the cell. Figure 2(a) shows ε^T (red data) and ε^B (black data) for particles swimming at $V_0 = 2$ μm/s. For large values of F, the particles sediment to the bottom substrate, although $(1-\varepsilon)$ is larger than in the case of "passive" Brownian microbeads [compare the inset of Fig. 2(a) with Fig. 1(b)]. One reason for the observed difference lies in the larger effective thermal energy of active colloids with long-time diffusion coefficient [32],

$$D_{eff} = \frac{k_B T_{eff}}{6\pi\eta R} = D_0 + V_0^2 \tau_R, \quad (3)$$

where k_B is the Boltzmann constant, η is the solvent viscosity, T_{eff} is an effective temperature, and D_0, τ_R, and V_0 are the translational diffusion coefficient, reorientation timescale, and self-propulsion velocity of the active colloids (the latter is here assumed equal to xy-swimming velocity). Hence, active colloids are "hotter" than their passive counterparts, i.e., their sedimentation lengths, $l_g = k_B T_{eff}/F$, are significantly larger (the values are reported in the Supplemental Material [30]). On the other hand, when $F \to 0$, accumulation is observed almost entirely at the top wall of the cell; this behavior cannot

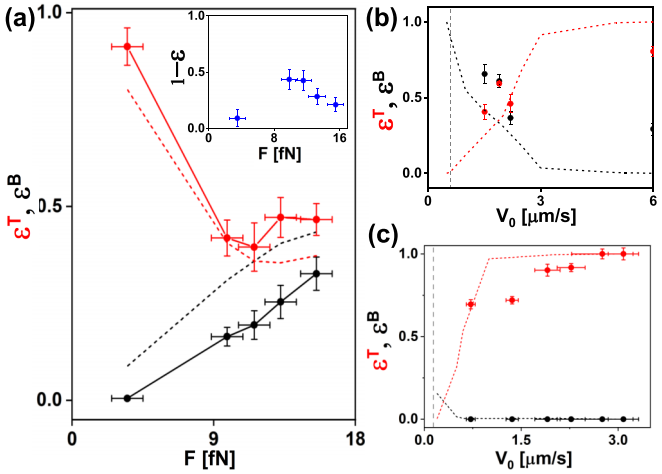

FIG. 2. (a) Ratio of particles found at the bottom (ε^{B}, black) and top (ε^{T}, red) walls of the cell after one hour, plotted as a function of the buoyant weight F, for $V_0 = 2$ μm/s. Inset: $1-\varepsilon$ plotted as function of F for comparison with Fig. 1(b). [(b), (c)] ε^{T} and ε^{B} vs V_0 for (b) $F = 15.52$ fN ($[\mathrm{D_2O}] = 0\%$) and (c) for $F = 3.51$ fN ($[\mathrm{D_2O}] = 100\%$). The dashed-vertical lines denote the velocity at which the buoyant weight is equal to the Stokes drag, $6\pi\eta R V_0$. The dotted lines are numerical simulations, as described in the main text.

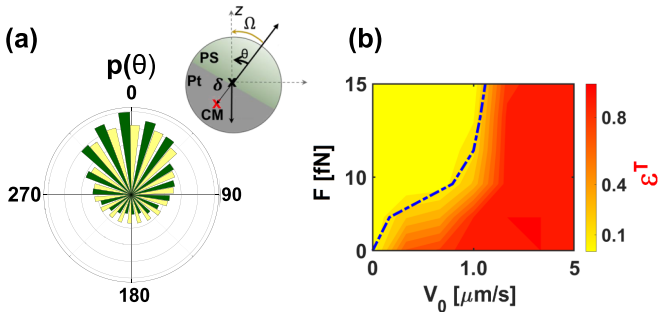

FIG. 3. (a) Normalized distribution $p(\theta)$ of the particle's orientation, θ, from numerical simulations at $V_0 = 2$ μm/s for $F = 15.52$ fN (yellow) and $F = 0$ fN (green). $\theta = 0$ corresponds to particles oriented antiparallel to gravity. Inset: Schematic representation of the model active particles used in simulations. As the particle is subjected to gravitational force, it experiences a torque $\boldsymbol{\Omega}$ that aligns the swimming velocity with the z axis. (b) Numerical results for the fraction of active particles at the top surface (ε^{T}) as a function of F and V_0. The dashed-blue line denotes the critical swimming velocity V_0^* for which $\varepsilon^{\mathrm{T}} = \varepsilon^{\mathrm{B}}$.

be rationalized neither by taking into account an effective diffusivity, which does not have a preferential direction, nor the persistence length, $L = V_0\tau_{\mathrm{R}}$, which is much smaller than the cell's height. Even in the event of l_{g} of the order or larger than the cell's height (small F, large V_0), one would expect $\varepsilon^{\mathrm{B}} \to 0.5$ and $\varepsilon^{\mathrm{T}} \to 0.5$. Thus, sedimentation-length arguments based on an effective diffusivity are not enough to explain the accumulation of active particles at the top wall. In Figs. 2(b) and 2(c), we plot ε^{B} and ε^{T} as a function of the swimming velocity for the limit cases of pure $\mathrm{H_2O}$-$\mathrm{H_2O_2}$ ($F = 15.52$ fN) and pure $\mathrm{D_2O} - \mathrm{H_2O_2}$ ($F = 3.51$ fN) mixtures. In water [Fig. 2(b)], slow particles sediment towards the bottom substrate and fast swimmers migrate to the top wall. The black and red data show a crossover at $V_0 \simeq 2$ μm/s, which is significantly larger than the velocity at which the buoyant weight is equal to the Stokes drag (dashed-vertical line). In contrast, pure deuterium oxide entirely favours levitation within our experimental range [Fig. 2(c)]. In the following, the critical velocity where ε^{T}=ε^{B} is denoted as V_0^* (see the Supplemental Material [30]).

The experimental data in Fig. 2 are fully rationalized by considering that the Pt-coated microparticles are bottom-heavy [20,23,24], i.e., they are subjected to a torque that favours a swimming direction against the gravitational field (*negative gravitaxis*). We employ overdamped Brownian dynamics simulations [33] where the patchy microswimmers are modelled as active Brownian disks equipped with translational velocity V_0 that points towards the pole of the uncoated hemisphere and rotates in the xz plane. Thermal fluctuations are included in both the translational and rotational motion. The disks are subjected to a buoyant weight $\mathbf{F}$ and experience a torque $\boldsymbol{\Omega}$ due to a point-like weight $\mathbf{F}_{\mathrm{Pt}} = 2\pi\lambda R^2\rho_{\mathrm{Pt}}\mathbf{g}$ ($\rho_{\mathrm{Pt}} = 21.45$ g/cm^3) located on the axis of the velocity vector at a distance $\delta \simeq 0.3R$ from the geometric center of the particle, as schematically illustrated in the inset of Fig. 3(a). $\boldsymbol{\Omega}$ tends to align the velocity vector with the z axis [Fig. 3(a)]. Importantly, the torque still exists even if $F \simeq 0$ and is in fact approximately constant for all values of $\mathbf{F}$ because platinum is much heavier than the solvent for any concentration of deuterium oxide. This is in stark contrast with existing studies of gravitactic bottom-heavy swimmers, in which the weight is varied using particles of different size [20,21]. The governing equations used for the simulations and a detailed description of the gravitational torque experienced by the particles are in the Supplemental Material [30].

In simulations, a particle is initially placed at a random height and self-propels in a rectangular box of height 1 mm until it reaches the top or bottom boundary, at which point the simulation ends and a contribution towards ε^{T} or ε^{B} is counted. If the particle has not reached any wall after the experimental time (one hour), it is considered to be in the bulk. This approach is motivated by the fact that, in experiments, active colloids rarely leave either of the walls due to self-generated hydrodynamic and chemical fields [14,26,29,34]. The process is repeated for $N = 10^4$ particles independently. We emphasize that the simulations do not include any free parameter; all values are taken from the experimental conditions (see Supplemental Material [30]).

In spite of the simplicity of the model, numerical and experimental results show good agreement [see dotted lines and symbols in Figs. 2(a)–2(c)]; a very pronounced negative gravitaxis takes place as the particles become, on average, density matched with the solvent, i.e., as F decreases [Fig. 2(a)]. For $F = 15.52$ fN and large V_0, we find more particles in bulk in experiments than in simulations, possibly due to a fraction of particles that are very slow. Even in presence of an aligning torque, there is a critical swimming velocity V_0^* below (above) which the particles migrate preferentially downwards (upwards) [Figs. 2(b) and 2(c)]. The experimental value of V_0^* is also shown as blue dashed line in Fig. 3(b), where we summarize the results by plotting the fraction of particles reaching the top surface as a function of both V_0 and F. V_0^* is within the region where the color changes, i.e.,

where particles equally accumulate on the top and bottom wall. Negative gravitaxis (red area) is achieved using "fast" or "light" microswimmers. V_0^* can be also predicted from the orientation distribution $p(\theta)$ by extracting the average upward velocity (see the Supplemental Material [30]).

The buoyant weight strongly affects not only the behavior of active particles in bulk fluids, but also their motion once they reach one of the flat walls. Existing experiments of catalytic colloids in $H_2O - H_2O_2$ suggest that the active motion near a flat wall is two dimensional both in terms of translation and rotation; the particles swim at constant distance from the surface with an angle between the orientation vector (i.e., the vector linking the poles of the two hemispheres) and the z axis that is given by the interplay between the wall-particle interaction torque and rotational diffusivity [14,15,26–28]. Interestingly, some experiments report an orientation vector perfectly parallel to the underlying substrate [26], while others suggest an inclination [14]. In the following, we briefly show that gravity significantly enriches this scenario.

We acquire z stacks of active colloids swimming near the bottom wall [one example is shown in Fig. 1(c), green line] using an inverted confocal microscope (Nikon, objective 60x Oil, NA = 1.4). Here, the cell consists of a Teflon ring glued on a microscope cover slide. z stacks of the particles near the bottom substrate are taken at 0.25 frames per second. In each z stack, we acquire 75 frames at 18 frames per second with a z step of 0.2 μm, which means that we scan a total distance of 15 μm from the bottom substrate. In the time interval $1/18 = 55$ ms, the particle moves less than 30 nm because of convection, diffuses over less than 100 nm, and rotates less than 5 degrees because of rotational Brownian motion. Figures 4(a) and 4(b) show the (3D) trajectories (extracted using a Python tracking package [35]) in $H_2O - H_2O_2$ mixtures ($F = 15.52$ fN) at $V_0 = 0.3$ μm/s and $V_0 = 0.6$ μm/s. Instead, the particle in Fig. 4(c) has the same swimming velocity as the one in Fig. 4(b), but about half its buoyant weight ($F = 9.8$ fN). In all situations, the particles are confined near the substrate but undergo an oscillatory motion in the z direction, even reaching maximum distances from the underlying wall larger than $7R$ [Fig. 4(c)].

From the trajectories, we calculate the instant velocity v in the xy plane as the distance traveled by the particle between two consecutive frames [Figs. 4(a)–4(c), orange curves]; note that V_0 is similar to $\langle v \rangle$ but not exactly the same because V_0 is an ensemble average). The noise level for the instantaneous velocities [see grey areas in Figs. 4(a)–4(c)] is about 50% considering that the colloids diffuse over about 1 μm within consecutive z stacks. We also measure the normalized fluorescence brightness I/I_0 of each active particle [Figs. 4(a)–4(c), green curves], where I_0 is the maximum brightness defined as the total intensity of a fully saturated circular region around the particle center and is measured using uncoated polystyrene particles of the same size. Both I and I_0 are extracted by looking at the intensities in different z planes and later interpolating to the focal plane. The particle's brightness is directly connected to its orientation, while being independent of its z position; a Pt cap that is oriented downwards, facing the glass substrate, screens the emitted fluorescence light, thus making the particle appear darker. Since the catalytic microswimmers move in the direction of the PS

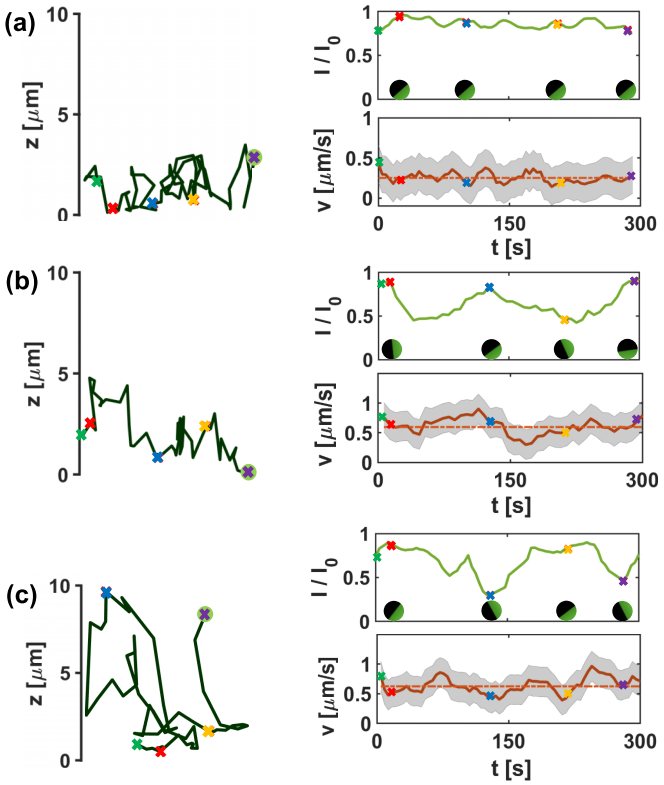

FIG. 4. Trajectories of active particles swimming on a glass substrate at (a) $V_0 = 0.3$ μm/s and [(b), (c)] $V_0 = 0.6$ μm/s for (a) and (b) $F = 15.52$ fN and (c) $F = 9.8$ fN. The graphs show the corresponding normalized brightness, I/I_0, and instant velocity v as a function of time (the horizontal-dashed lines denote the average velocity of the particles). The coloured crosses mark the same times. The circles below the green curves are sketches of the active particles seen transversally in the sample, as if the x axis were the bottom wall. The black and green semicircles correspond to the Pt-cap and the uncoated hemisphere, respectively.

hemispheres, the combination of v and I/I_0 gives us access to the dynamics of the particles as it navigates on the substrate; small values of I/I_0 correspond to particles swimming upwards [e.g., blue cross in Fig. 4(c)], whereas the simultaneous observation of large I/I_0 and small v suggests that the swimmer is temporarily pushing against the wall [e.g., red cross in Fig. 4(c)]. The largest values of v are measured when the active colloids swim parallel to the wall. The orientation of "slow" and "heavy" particles [Fig. 4(a)] is predominantly fixed, although it slightly oscillates in z with period $T \sim 58$ s, where T is extracted from the frequency of the first peak of the power spectral density of the fluorescence intensity signal (see the Supplemental Material [30]). T becomes much larger for faster [Fig. 4(b), $T \sim 128$ s] and lighter [Fig. 4(c), $T \sim 148$ s] colloids, suggesting that gravity plays an important role in the rotational and translational motion of active swimmers near flat walls.

Oscillatory active trajectories above a flat confinement have been attributed to a repulsive potential between the flat confinement and the particle [36]. The key ingredients are: Self-propulsion, short-ranged particle-wall repulsion, and phoretic and hydrodynamic interactions. Here the scenario is even more complex because of bottom heaviness and the

different interaction of the coated and uncoated hemispheres with the underlying negatively charged surface. Nonetheless, the z oscillations shown in Fig. 4 occur at timescales that are much larger than τ_R as well as the characteristic relaxation time of the torque in bulk, suggesting that the particle-wall interactions—which are more pronounced for "heavy" particles swimming closer to the substrate—play a pivotal role in determining the reorientation of the colloids in z. The oscillatory motion in z (Fig. 4) and the 2D ABM model used to extract the xy swimming velocity V_0 (see Supplemental Material [30]) are also seemingly contradictory. However, the approach used in the Supplemental Material [30] is justified by the fact that, in our experiments, the timescale of z oscillations (T) is much larger than the characteristic reorientation time in the xy plane (τ_R).

To summarize, we investigated the active motion of catalytic colloids as a function of their buoyant weight F, and swimming velocity V_0. Our results lead to two main conclusions. (1) Weightlessness is not easy to achieve in suspensions of patchy self-propelling particles; gravitational torques caused by the different density of the two hemispheres favor the migration towards the top boundary even when the average buoyant weight is zero. (2) The reorientation of catalytic microswimmers near flat walls—thus their quasi-two-dimensional motion—strongly depends on F and V_0, far beyond what has been reported to date. Further studies will address the role of friction in active matter systems; we envisage that, due to 3D reorientation, active colloids will experience a fluctuating friction coefficient as they roam on rough substrates.

We thank Juliane Simmchen and Hartmut Löwen for inspiring discussions. We are also grateful to Carolina van Baalen for helping us sputter-coat the particles, and Stefan Egelhaaf and Patrick Laermann for the access to the confocal microscope.

[1] C. Bechinger, R. DiLeonardo, H. Löwen, C. Reichhardt, G. Volpe, and G. Volpe, Active particles in complex and crowded environments, Rev. Mod. Phys. **88**, 045006 (2016).

[2] S. Ramaswamy, The mechanics and statistics of active matter, Annu. Rev. Condens. Matter Phys. **1**, 323 (2010).

[3] S. J. Ebbens and J. R. Howse, In pursuit of propulsion at the nanoscale, Soft Matter **6**, 726 (2010).

[4] M. You, C. Chen, L. Xu, F. Mou, and J. Guan, Intelligent micro/nanomotors with taxis, Acc. Chem. Res. **51**, 3006 (2018).

[5] J. Katuri, X. Ma, M. M. Stanton, and S. Sánchez, Designing micro-and nanoswimmers for specific applications, Acc. Chem. Res. **50**, 2 (2017).

[6] D. Xu, Y. Wang, C. Liang, Y. You, S. Sanchez, and X. Ma, Self-propelled micro/nanomotors for on-demand biomedical cargo transportation, Small **16**, 1902464 (2020).

[7] J. Zhang, E. Luijten, B. A. Grzybowski, and S. Granick, Active colloids with collective mobility status and research opportunities, Chem. Soc. Rev. **46**, 5551 (2017).

[8] A. Morin, J.-B. Caussin, C. Eloy, and D. Bartolo, Collective motion with anticipation: Flocking, spinning, and swarming, Phys. Rev. E **91**, 012134 (2015).

[9] J. Palacci, S. Sacanna, A. P. Steinberg, D. J. Pine, and P. M. Chaikin, Living crystals of light-activated colloidal surfers, Science **339**, 936 (2013).

[10] I. Buttinoni, J. Bialké, F. Kümmel, H. Löwen, C. Bechinger, and T. Speck, Dynamical Clustering and Phase Separation in Suspensions of Self-Propelled Colloidal Particles, Phys. Rev. Lett. **110**, 238301 (2013).

[11] J. L. Anderson, Colloid transport by interfacial forces, Annu. Rev. Fluid Mech. **21**, 61 (1989).

[12] A. Aubret, S. Ramananarivo, and J. Palacci, Eppur si muove, and yet it moves: Patchy (phoretic) swimmers, Curr. Opin. Colloid Interface Sci. **30**, 81 (2017).

[13] J. R. Howse, R. A. L. Jones, A. J. Ryan, T. Gough, R. Vafabakhsh, and R. Golestanian, Self-Motile Colloidal Particles: From Directed Propulsion to Random Walk, Phys. Rev. Lett. **99**, 048102 (2007).

[14] K. Dietrich, D. Renggli, M. Zanini, G. Volpe, I. Buttinoni, and L. Isa, Two-dimensional nature of the active Brownian motion of catalytic microswimmers at solid and liquid interfaces, New J. Phys. **19**, 065008 (2017).

[15] S. Ketzetzi, J. de Graaf, R. P. Doherty, and D. J. Kraft, Slip Length Dependent Propulsion Speed of Catalytic Colloidal Swimmers near Walls, Phys. Rev. Lett. **124**, 048002 (2020).

[16] A. Brown and W. Poon, Ionic effects in self-propelled pt-coated Janus swimmers, Soft Matter **10**, 4016 (2014).

[17] J. Palacci, C. Cottin-Bizonne, C. Ybert, and L. Bocquet, Sedimentation and Effective Temperature of Active Colloidal Suspensions, Phys. Rev. Lett. **105**, 088304 (2010).

[18] R. Keßler, D. Bräuer, C. Dreißigacker, J. Drescher, C. Lozano, C. Bechinger, P. Born, and T. Voigtmann, Direct-imaging of light-driven colloidal Janus particles in weightlessness, Rev. Sci. Instrum. **91**, 013902 (2020).

[19] N. Sakaï and C. P. Royall, Active dipolar colloids in three dimensions: Strings, sheets, labyrinthine textures and crystals, arXiv:2010.03925.

[20] A. I. Campbell and S. J. Ebbens, Gravitaxis in spherical Janus swimming devices, Langmuir **29**, 14066 (2013).

[21] A. I. Campbell, R. Wittkowski, B. ten Hagen, H. Löwen, and S. J. Ebbens, Helical paths, gravitaxis, and separation phenomena for mass-anisotropic self-propelling colloids: Experiment versus theory, J. Chem. Phys. **147**, 084905 (2017).

[22] B. Ten Hagen, F. Kümmel, R. Wittkowski, D. Takagi, H. Löwen, and C. Bechinger, Gravitaxis of asymmetric self-propelled colloidal particles, Nat. Commun. **5**, 4829 (2014).

[23] M. Enculescu and H. Stark, Active Colloidal Suspensions Exhibit Polar Order under Gravity, Phys. Rev. Lett. **107**, 058301 (2011).

[24] H. Stark, Swimming in external fields, Eur. Phys. J.: Spec. Top. **225**, 2369 (2016).

[25] F. Ginot, A. Solon, Y. Kafri, C. Ybert, J. Tailleur, and C. Cottin-Bizonne, Sedimentation of self-propelled Janus colloids: Polarization and pressure, New J. Phys. **20**, 115001 (2018).

[26] S. Das, A. Garg, A. I. Campbell, J. Howse, A. Sen, D. Velegol, R. Golestanian, and S. J. Ebbens, Boundaries can steer active Janus spheres, Nat. Commun. **6**, 8999 (2015).

[27] S. Ketzetzi, J. de Graaf, and D. J. Kraft, Diffusion-Based Height Analysis Reveals Robust Microswimmer-Wall Separation, Phys. Rev. Lett. **125**, 238001 (2020).

[28] S. Das, Z. Jalilvand, M. N. Popescu, W. E. Uspal, S. Dietrich, and I. Kretzschmar, Floor-or ceiling-sliding for chemically active, gyrotactic, sedimenting Janus particles, Langmuir **36**, 7133 (2020).

[29] W. Uspal, M. N. Popescu, S. Dietrich, and M. Tasinkevych, Self-propulsion of a catalytically active particle near a planar wall: From reflection to sliding and hovering, Soft Matter **11**, 434 (2015).

[30] See Supplemental Material at http://link.aps.org/supplemental/10.1103/PhysRevResearch.5.L012018 for details in methods and simulation.

[31] P. Giguère and O. Maass, The heterogeneous catalytic decomposition of hydrogen peroxide in heavy water, Can. J. Res. **18b**, 84 (1940).

[32] B. ten Hagen, S. van Teeffelen, and H. Löwen, Brownian motion of a self-propelled particle, J. Phys.: Condens. Matter **23**, 194119 (2011).

[33] A. Callegari and G. Volpe, Numerical simulations of active Brownian particles, in *Flowing Matter*, edited by F. Toschi and M. Sega (Springer International Publishing, Cham, 2019), pp. 211–238.

[34] M. N. Popescu, W. E. Uspal, A. Dominguez, and S. Dietrich, Effective interactions between chemically active colloids and interfaces, Acc. Chem. Res. **51**, 2991 (2018).

[35] D. B. Allan, T. Caswell, N. C. Keim, C. M. van der Wel, and R. W. Verweij, soft-matter/trackpy: Trackpy v0.5.0, Zenodo (2024), doi:10.5281/zenodo.4682814.

[36] P. Bayati, M. N. Popescu, W. E. Uspal, S. Dietrich, and A. Najafi, Dynamics near planar walls for various model self-phoretic particles, Soft Matter **15**, 5644 (2019).